Drivers and Reversibility of Abrupt Ocean State Transitions in the Amundsen Sea, Antarctica

Justine Caillet, Nicolas C Jourdain, Pierre Mathiot, Hartmut H Hellmer, Jérémie Mouginot

JGR Oceans

RESEARCH ARTICLE
10.1029/2022JC018929

Drivers and Reversibility of Abrupt Ocean State Transitions in the Amundsen Sea, Antarctica

Justine Caillet[1], Nicolas C. Jourdain[1], Pierre Mathiot[1], Hartmut H. Hellmer[2], and Jérémie Mouginot[1]

[1]Université Grenoble Alpes, CNRS, IRD, Grenoble INP, IGE, Grenoble, France, [2]Alfred Wegener Institute Helmholtz Centre for Polar and Marine Research, Bremerhaven, Germany

Key Points:

- The currently warm ice-shelf cavities of the Amundsen sector could become or have been cold for slightly colder climatic conditions
- The transitions are reversible: canceling the atmospheric perturbation brings the ocean back to its unperturbed state within a few decades
- All the transitions are primarily driven, at multi-decadal scale, by changes in surface buoyancy fluxes over the continental shelf

Supporting Information:

Supporting Information may be found in the online version of this article.

Correspondence to:

J. Caillet,
justine.caillet@univ-grenoble-alpes.fr

Citation:

Caillet, J., Jourdain, N. C., Mathiot, P., Hellmer, H. H., & Mouginot, J. (2023). Drivers and reversibility of abrupt ocean state transitions in the Amundsen Sea, Antarctica. *Journal of Geophysical Research: Oceans*, *128*, e2022JC018929. https://doi.org/10.1029/2022JC018929

Received 2 JUN 2022
Accepted 15 NOV 2022

Abstract Ocean warming around Antarctica has the potential to trigger marine ice-sheet instabilities. It has been suggested that abrupt and irreversible cold-to-warm ocean tipping points may exist, with possible domino effect from ocean to ice-sheet tipping points. A 1/4° ocean model configuration of the Amundsen Sea sector is used to investigate the existence of ocean tipping points, their drivers, and their potential impact on ice-shelf basal melting. We apply idealized atmospheric perturbations of either heat, freshwater, or momentum fluxes, and we characterize the key physical processes at play in warm-to-cold and cold-to-warm climate transitions. Relatively weak perturbations of any of these fluxes are able to switch the Amundsen Sea to an intermittent or permanent cold state, that is, with ocean temperatures close to the surface freezing point and very low ice-shelf melt rate. The transitions are reversible, that is, canceling the atmospheric perturbation brings the ocean system back to its unperturbed state within a few decades. All the transitions are primarily driven by changes in surface buoyancy fluxes resulting from the freshwater flux perturbation or from modified net sea-ice production due to either heat flux or sea-ice advection anomalies. These changes affect the vertical ocean stratification over the continental shelf and thereby the eastward undercurrent at the shelf break, which both impact ice-shelf melting. As sea-ice induced deep convection is already quite limited in present-day conditions, surface buoyancy gain in a warmer climate has relatively little effect on deep ocean properties compared to colder climate conditions.

Plain Language Summary The West Antarctic Ice Sheet is under the threat of a partial collapse, which would induce rapid global sea level rise. This threat is partly related to the thinning of floating ice shelves, and the consequent retreat of the grounding line, which is a self-sustained ice dynamics process. It is triggered by increased basal melting of the ice shelves, which results from enhanced flow of relatively warm waters onto the continental shelf. It has been suggested that self-sustained ocean processes may lead to abrupt changes in the flow of warm water into ice-shelf cavities, which could facilitate the tipping to a marine ice-sheet instability. Here, we analyze whether such abrupt ocean changes can occur under cold-to-warm or warm-to-cold transitions in the Amundsen Sea, West Antarctica. We use a regional ocean model with a set of idealized local atmospheric perturbations to characterize the thresholds and reversibility of ocean abrupt changes.We find that the currently warm Amundsen Sea could switch intermittently or permanently to a cold state for relatively weak atmospheric perturbations and could be slightly warmer in the future. All transitions are reversible. The main mechanism involved on decadal scale is related to a change in the surface buoyancy fluxes.

1. Introduction

The West Antarctic Ice Sheet has lost mass over the last few decades and has thus contributed significantly to global sea level rise. Warming of the oceanic sub-surface seems to have caused an increase in melting under floating ice shelves, particularly in the Amundsen Sea (Jenkins et al., 2018). Depending on the bedrock slope direction (Pattyn et al., 2012; Schoof, 2007) and ice-shelf lateral buttressing (Gudmundsson, 2013), a sufficiently strong and persistent increase in basal melting can lead to a marine ice-sheet instability (MISI), resulting in a self-sustained retreat of the glacier's grounding line and to the acceleration of its flow (Favier et al., 2014; Joughin et al., 2014).

Instabilities are triggered above a certain level of ocean warming (critical threshold or tipping point), with the possible existence of multiple thresholds. Thus, Rosier et al. (2021) estimated that Pine Island Glacier would undergo a MISI and major mass loss for an oceanic warming of +1.2°C relative to the present. Garbe et al. (2020) estimated that a tipping point of +2°C global warming relative to preindustrial could cause a MISI of the entire

West Antarctic Ice Sheet. Tipping points are characterized by a hysteresis, that is, restoring the forcing to before the occurrence of the tipping point is not sufficient to restore the system to its original state. Identifying these tipping points precisely and linking them to climate projections would allow the effects of future rapid sea level rise to be anticipated and possibly mitigated (Durand et al., 2022; Hinkel et al., 2019).

The abrupt nature of these ice tipping points in West Antarctica could be enhanced if ocean warming itself were subject to a tipping point. This would be a cascading tipping point, or domino effect (Brovkin et al., 2021; Dekker et al., 2018; Wunderling et al., 2021). It has been suggested, that beyond a certain threshold of melting, the Greenland Ice Sheet could induce a sudden weakening of the Atlantic Meridional Overturning Circulation, which, in turn, would lead to ocean warming around Antarctica (Turney et al., 2020; Wunderling et al., 2021).

Another type of oceanic tipping point has been highlighted in the Weddell Sea (Hellmer et al., 2012, 2017). Reduced sea-ice formation under continued global warming, a freshening of the continental shelf, and increased ocean surface stress could cause the slope current to diverge in the southeast Weddell Sea. The reorientation would facilitate the entry of Warm Deep Water, a cooler variant of Circumpolar Deep Water (CDW), onto the continental shelf and significantly increase basal melting, which would lead to a self-reinforcing process due to the injection of meltwater. The process is irreversible with the twentieth-century atmospheric forcing: only an imposed decrease in basal melt rate can hinder the self-sustaining process.

The Amundsen Sea environment is very different as cavities are already relatively warm (Jacobs et al., 1996, 2012). Paleoclimatic indicators suggest that the entire Amundsen continental shelf was covered by an ice sheet (either grounded or floating) at the Last Glacial Maximum (Larter et al., 2014). A particularly large retreat of the ice-sheet front and grounding line occurred between 20,000 and 10,000 years BP (Larter et al., 2014), with further smaller retreats occurring thereafter, notably around 1945 and 1970 (Smith et al., 2017). Ocean temperatures and warming rates during these transitions are not known, but it is possible that oceanic tipping points similar to those reported by Hellmer et al. (2012, 2017) for the Weddell Sea occurred in the Amundsen Sea area as well.

In this paper, we analyze under which atmospheric forcing conditions warm-to-cold, cold-to-warm, and warm-to-warmer ocean transitions in the Amundsen Sea have occurred or could occur, and we test the reversibility of these transitions, that is, the presence of hysteresis. We use a regional ocean modeling approach with a set of idealized atmospheric perturbations.

2. Materials and Methods

2.1. Model and Configuration

The Nucleus for European Modeling of the Ocean (NEMO) model, version 3.6, including the OPA ocean model (Madec & the NEMO Team, 2016) and the Louvain-la-Neuve sea-ice model LIM-3.6 (Rousset et al., 2015), is used in a regional configuration of the Amundsen Sea (Figure 1). Our model parameters are similar to Jourdain et al. (2019), with a representation of ice–ocean exchange beneath static ice shelves, with melt rate depending on ocean velocity, temperature and salinity (Jourdain et al., 2017; Mathiot et al., 2017), and barotropic tides prescribed as lateral boundary conditions from seven constituents of the FES2012 tidal model (Carrère et al., 2012; Lyard et al., 2006).

Compared to Jourdain et al. (2019), the domain is slightly extended, now covering from 142°W to 85°W and from 76.3°S to 59.8°S, and the resolution is reduced to 1/4° in longitude, that is, a quasi-isotropic resolution ranging from 14 km at the northern boundary to 6.5 km in the southernmost part of the domain. Bathymetry, as well as surface and lateral boundary conditions also differ from Jourdain et al. (2019) and cover the period 1958–2018 in this study. The period 1958–1968 is left for spin-up and discarded in our analyses.

The bathymetry and ice-shelf draft interpolated on the model grid are from the second version of the BedMachine Antarctica dataset (Morlighem et al., 2020). This recent dataset represents Thwaites Ice Shelf after its partial collapse. The B22A iceberg as well as other very large tabular icebergs, absent from BedMachine Antarctica, are represented as static flat ice shelves. Their horizontal shape and location are derived from a MODIS-visible image (provided by the US National Snow and Ice Data Center) taken on September 5, 2003. The depth of the B22A iceberg base was calculated as $D = H\rho_w/(\rho_w - \rho_i)$, where ρ_w is the seawater density (1,027 kg m^{-3}), ρ_i the iceberg density (917 kg m^{-3}), and H the freeboard that is 40.8 m on average for B22A in the altimetry dataset

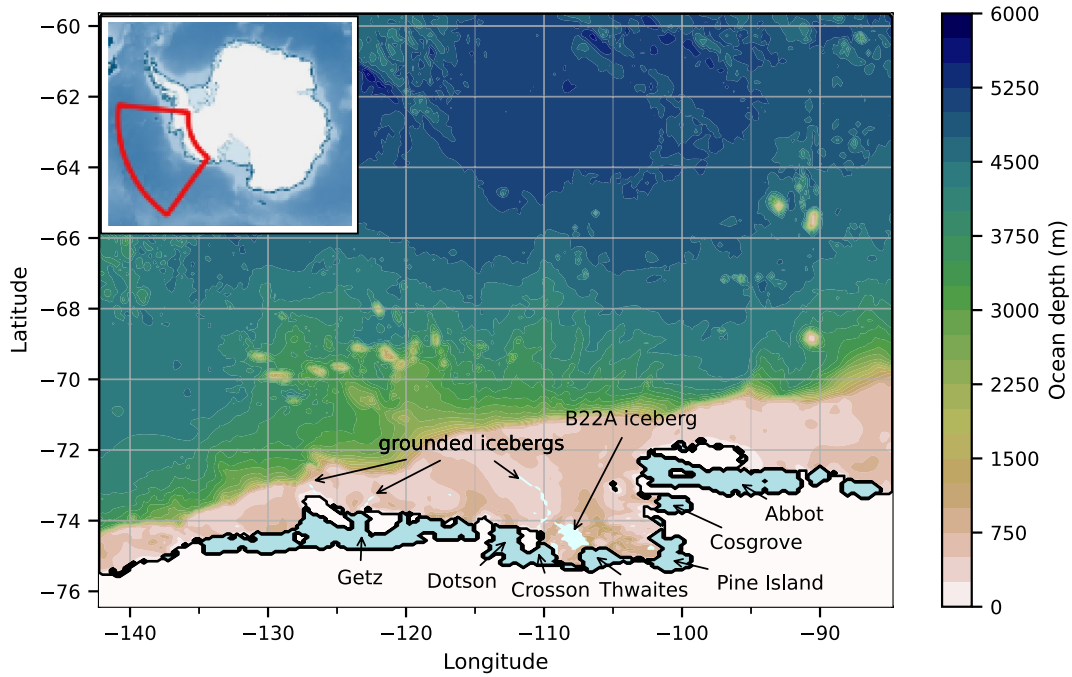

Figure 1. Used regional configuration of the Amundsen Sea. Bathymetry and ice-shelf draft are from the second version of the BedMachine Antarctica dataset (Morlighem et al., 2020). Grounded ice is shaded in white, ice shelves are colored in blue, and main tabular icebergs in light cyan. The general view is drawn from the geospatial data package Quantarctica (Matsuoka et al., 2021).

of Tournadre et al. (2015). The resulting estimated depth is approximately 380 m, which we apply to the smaller tabular icebergs that are absent from the altimetry dataset. We then assume that these icebergs behave like flat ice shelves if the bathymetry is deeper than 380 m plus two ocean model vertical levels (the minimum water column thickness in NEMO) and like an island (i.e., no water column) if the bathymetry is shallower. The huge B22A iceberg calved from the Thwaites ice tongue in 2002 and has drifted very slowly since then (Antarctic Iceberg Tracking Database, Budge & Long, 2018). A similar calving event occurred in the late 1960s (Lindsey, 1995). The resulting iceberg was eventually designated B10 in 1992 when it started a 15-year drift across the Amundsen Sea before breaking up and drifting further away (Budge & Long, 2018). Numerous smaller icebergs regularly drift westward in the Amundsen Sea and ground on the eastern flank of bathymetric ridges shallower than approximately 400 m (Mazur et al., 2017). We therefore artificially place a wall along the 380 m isobath on the eastern flank of Bear Ridge (in a similar way as Bett et al., 2020), north of Siple Island, and on the main ridge in between. These permanent lines of grounded icebergs were shown to favor the formation of polynyas with impact on ice-shelf melting (Bett et al., 2020; Nakayama et al., 2014).

The conditions at the lateral ocean and sea-ice boundaries are derived from the 5-day mean outputs of a global simulation very similar to the one described in Merino et al. (2018) except that it is spun up from 1958 and that the imposed ice-shelf melt flux increases linearly from 1990 to 2005 and is constant before and after that, with values corresponding to the FRESH+ and FRESH− reconstructions of Merino et al. (2018). Here, the temperature and salinity boundary conditions are corrected by the difference between the seasonal climatology of the World Ocean Atlas 2018 (WOA18) database (Garcia et al., 2019) and the seasonal climatology of the global simulation. The global simulation used for boundary conditions represents melting of Lagrangian icebergs (Merino et al., 2016), and the corresponding 5-day mean melt fluxes are applied as a freshwater flux at the surface of our regional configuration. The atmospheric forcing data are taken from the JRA55-do reanalysis (Tsujino et al., 2018) between 1958 and 2018. The fluxes between ocean (or sea ice) and atmosphere are calculated using the CORE bulk formulae described in Griffies et al. (2009) and Large and Yeager (2004).

As Supporting Information, we present a few model experiments that were used to explore the sensitivity to some model parameters (methodology in Section S2 in Supporting Information S1). A "reference configuration" was selected (Sections S6 and S7 in Supporting Information S1) based on its fidelity in terms of sea ice

extent variability (Section S3 in Supporting Information S1), temperature and salinity stratification (Section S4 in Supporting Information S1), and ice shelf basal melt rates (Section S5 in Supporting Information S1). The atmospheric forcing fields are perturbed (Section 2.2) to investigate ocean tipping points.

2.2. Atmospheric Forcing Perturbations

In the following, we investigate three pathways to induce ocean tipping points in the Amundsen Sea through surface flux modifications of either heat, freshwater, or momentum. We decided to consider idealized atmospheric perturbations in order to identify and isolate the processes at play. Thus, each surface flux is perturbed independently. Our perturbations are bounded by typical conditions of the Last Glacial Maximum, that is, down to −10°C globally relative to the current surface air temperature (Masson-Delmotte et al., 2010), and by typical projections at 2,300 under the SSP5-8.5 scenario, that is, up to +10°C of global warming from the current situation (Lee et al., 2021). Climate simulations indicate that the air temperature in the Amundsen Sea rises approximately as much as the global mean temperature, at least from 2,000 to 2,200 (Collins et al., 2013, their Figure 12.10). We therefore assume that the Amundsen Sea air temperatures vary uniformly from −10°C to +10°C, although this likely neglects polar feedbacks that may become significant for our most extreme perturbations.

The heat flux is perturbed through air temperature within the aforementioned bounds. To limit the impact of this perturbation on evaporation, and thus on the freshwater flux, specific humidity e is also modified to keep the difference between e and the saturation specific humidity e_s unchanged. In other words, we perturbate the sensible heat flux but not the latent heat flux. The modified specific humidity $e(T+\Delta T)$ is calculated through the Magnus empirical fit of the Clausius Clapeyron law (e.g., Donat-Magnin et al., 2021), here expressed with e in hPa and T in degree Celsius:

$$\begin{cases} e_s(T) = 6.1094 \exp\left(\dfrac{17.625\,T}{T + 243.04}\right) \\ e_s(T+\Delta T) \approx e_s(T) \exp\left(\dfrac{17.625\,\Delta T}{T + 243.04}\right) \\ e(T+\Delta T) = e(T) + e_s(T+\Delta T) - e_s(T) \end{cases} \quad (1)$$

For the freshwater flux, we decide to modify precipitation while maintaining the ratio between solid and liquid precipitation for the sake of simplicity (the heat flux associated with snow melting in the ocean is relatively low). Precipitation near Antarctica has been shown to evolve following the Clausius-Clapeyron law (Donat-Magnin et al., 2021; Ligtenberg et al., 2013). The range of variation is therefore indexed to the temperature range considered for the heat flux: precipitation is multiplied by factors between 0.48 and 1.99, corresponding to coldest (−10°C) and warmest (+10°C) climatic conditions, respectively.

Ice shelf basal melting highly depends on whether the perturbations are applied only on the continental shelf or on the continental shelf and slope (not shown). We decided to include the continental slope in the perturbed area as this area is relevant for CDW intruding onto the shelf. The ice-shelf melt rates are not sensitive to further northward extension of the perturbation area, which indicates some robustness of our methodology. For the heat and freshwater flux perturbations, a transition area of 3° in latitude (about 340 km) and 4° in longitude limits the temperature and precipitation gradient, and thus the formation of strong density gradients, between the perturbed and unperturbed areas (Figure 2a).

The momentum flux is perturbed through meridional shifting of winds. To maintain flux independence, only the wind involved in the momentum flux calculation (i.e., ocean and sea-ice surface friction) is modified, while we keep the wind seen by latent and sensible heat fluxes unchanged in the bulk formulae. The applied wind shift ranges between a 4.7° northward shift for coldest (−10°C) climatic conditions (Gray et al., 2021) and a 4.7° southward shift for warmest (+10°C) conditions (extrapolated from the 2100 CMIP5-RCP8.5 sensitivity described in Spence et al., 2014, their Figure S3).

The momentum flux perturbation is also applied on the continental shelf and over the shelf break, and we put a coastal transition area of 150 km width between the perturbed wind and the katabatic winds near the ice-sheet

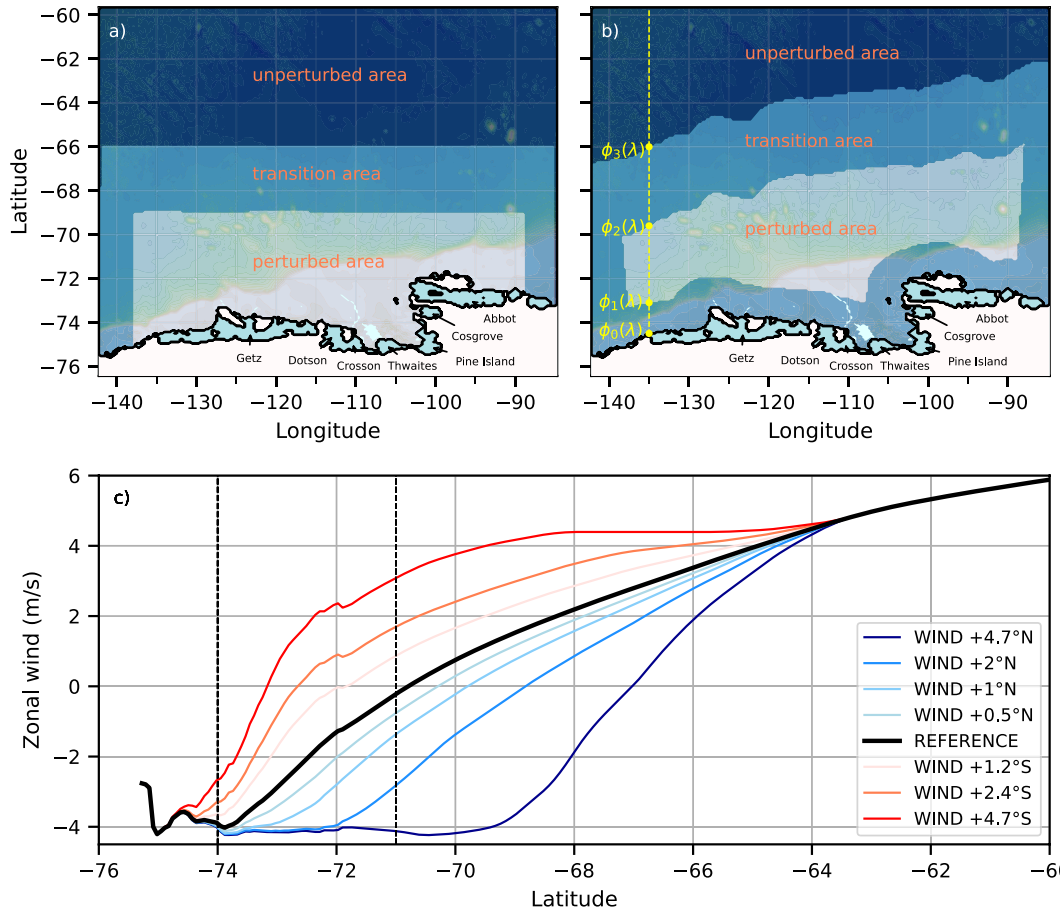

Figure 2. Location of the perturbed area (a) for heat and freshwater fluxes and (b) for momentum flux. The perturbed area is highlighted in light blue, the transition area in blue, and the unperturbed area in dark blue. The transition area avoids the artificial formation of strong density gradient or stress curl. (c) Zonal wind averaged between 100°W and 130°W for the momentum flux perturbations. The shelf break is located in between the two dashed vertical lines.

edges to avoid creating a substantial artificial wind curl perturbation (Figure 2b). The perturbed wind u at longitude and latitude (λ, ϕ) for a prescribed shift $\Delta\phi$ (positive northward) is calculated as follows:

$$\begin{cases} u(\lambda,\phi) = u(\lambda, \phi - \delta\phi) \\ \text{with :} \\ \delta\phi \quad = \dfrac{\phi - \phi_0(\lambda)}{\phi_1(\lambda) - \phi_0(\lambda)}\,\Delta\phi & \text{if } \phi_0(\lambda) \le \phi < \phi_1(\lambda) \\ \quad = \min(\Delta\phi, \phi - \phi_i(\lambda)) & \text{if } \phi_1(\lambda) \le \phi < \phi_2(\lambda) \\ \quad = \dfrac{\phi_3(\lambda) - \phi}{\phi_3(\lambda) - \phi_2(\lambda)}\,\Delta\phi & \text{if } \phi_2(\lambda) \le \phi < \phi_3(\lambda) \\ \quad = 0 & \text{if } \phi \ge \phi_3(\lambda) \end{cases} \tag{2}$$

where $\phi_{0\text{–}3}(\lambda)$ are shown in Figure 2b, $\phi_i(\lambda) = \phi_0(\lambda)$ or $\phi_i(\lambda) = \phi_3(\lambda)$ for a northward or southward shift, respectively. Next to the eastern and western domain boundaries, $\delta\phi$ has a linear transition to zero to ensure consistent wind forcing and prescribed ocean lateral boundary conditions. The perturbed zonal winds are shown in Figure 2c.

For the three types of perturbations, we conduct simulations with intermediate perturbations between the coldest and warmest climate perturbations in order to better characterize potential tipping points. Perturbations are

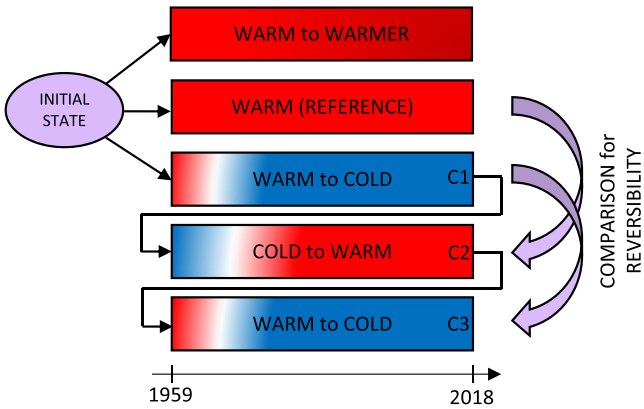

Figure 3. Simulation set-up. The annotations C1, C2, and C3 correspond to the first, second and third simulation cycle, respectively. The warm-to-warmer, warm-to-cold (C1), and cold-to-warm simulations enable us to identify the possible existence of transitions and the atmospheric conditions under which they occur. The cold-to-warm (C2) and warm-to-cold (C3) simulations are used to study their reversibility.

local, only applied on continental shelf and slope. We do not perturb lateral boundary conditions, that is, we maintain the presence of CDW in front of the continental shelf in all our simulations. It seems clear that cold conditions would prevail if CDW stopped to exist, and it is more interesting to identify how warm-to-cold abrupt transitions could occur in the presence of CDW.

2.3. Simulations

In order to assess the model response to atmospheric perturbations, we run 61-year simulations over the period 1958–2018. The simulation length is a compromise between computational cost and the description of the natural decadal variability of the ocean system, which can potentially impact the system stability and the occurrence of tipping points. The reference experiment corresponds to the configuration retained after calibration (see Supporting Information S1) with natural atmospheric and oceanic forcing over the modeled period. The model calibration improves the fidelity of the reference simulation although the interannual variability is smaller than expected (consequences will be discussed in Section 4).

The model spin-up is achieved after 10 years, thus, time series are only analyzed for the period 1968–2018. Most of our analyses are done for averages over the period 1988–2018, which overcomes the limited reliability of reanalyses before 1979 (G. J. Marshall et al., 2022), although we did not observe any specific behavior over this period in regard to the response to the perturbations.

The perturbed runs are identical to the reference run except for the atmospheric forcing. We study three possible types of transition: cold-to-warm transitions as reported by Hellmer et al. (2012, 2017) for the Weddell Sea, warm-to-cold and warm-to-warmer transitions related to ancient or distant future climate transitions. When an abrupt ocean transition occurs, reversibility is studied, that is, for cold-to-warm (C2 in Figure 3) and warm-to-cold transitions (C3 in Figure 3).

3. Results

3.1. Description of the Transitions and Their Reversibility

For the sake of clarity, this section focuses on the mean melt rate of Pine Island and Thwaites on the one hand, and of Crosson and Dotson ice shelves on the other hand. Cosgrove and Getz ice shelves undergo similar melt transitions, albeit with much lower and higher mean melt values, respectively (not shown).

For Pine Island–Thwaites, the heat flux perturbations lead to a permanent collapse of ice-shelf melting for air cooled by 2.5°C or more, with average melt rates below 0.3 m.w.e. yr^{-1} (meters of water equivalent per year, i.e., 1 m.w.e. yr^{-1} = 1,000 kg m^2 yr^{-1}), comparable to those experienced by the Ronne or Eastern Ross ice shelves (Rignot et al., 2013) (Figure 4a). The −1°C perturbation leads to a collapse of melt rates after year 2000, while the −0.5°C perturbation keeps relatively high melt rates. Cycling our simulations by repeating the period 1958–2018 indicates that the cooler state over 2000–2018 is related to the forcing data and not to a slow drift of our regional system as melt rates are again high before 2000 in the repeated simulations (not shown). The heat flux perturbations associated with higher air temperatures lead to a limited increase in basal melt rates, with no more than a 34% increase for the +10°C perturbation. The effect of increasing air temperatures seems to saturate, with little differences between +2°C and +10°C warming. Basal melt rates beneath Crosson–Dotson show a similar behavior as Pine Island–Thwaites, with intermittent periods of very low melt rates for perturbations as small as −0.5°C, permanent collapse of melt rates below −2.5°C (melt rate is slightly higher than that of Pine Island–Thwaites with typical values of 0.8–1.0 m.w.e. yr^{-1}), and a 28% increase in melt rates for +10°C (Figure 5a). It can also be noted that the amplitude of the seasonal melt cycle increases in response to warm perturbations for Pine Island–Thwaites but not for Crosson–Dotson.

The freshwater flux perturbations associated with lower precipitation lead to intermittent reductions in melt rates for precipitation reduced by 30% or more for Pine Island–Thwaites (Figure 4b). Particularly low melt rates are

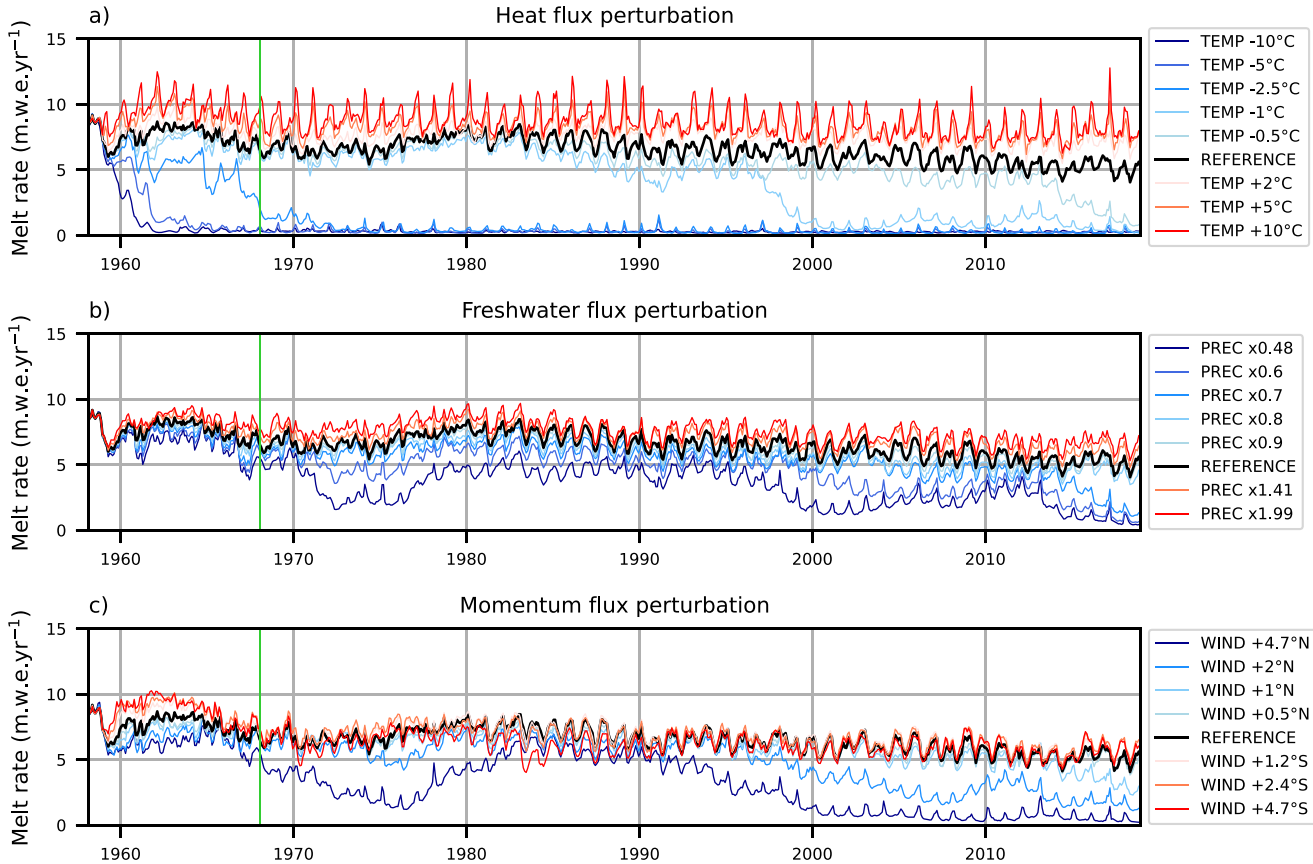

Figure 4. Evolution of monthly basal melting for Pine Island and Thwaites ice shelves over the period 1958–2018 for perturbations of (a) heat flux, (b) freshwater flux, and (c) momentum flux. The black curve (reference curve) corresponds to the simulation with the JRA55 reanalysis without modification. The red and blue curves correspond to simulations with atmospheric perturbations that aim to increase and decrease basal melting, respectively. The vertical green line indicates the end of the 10-year spin up.

found in the mid-1970s, early 2000s, and late 2010s, but never reach the extremely low values resulting from the heat flux perturbations. This contrasts with Crosson–Dotson for which extended periods of very low melt rates (below 1.1 m.w.e. yr^{-1}) are found when precipitation is reduced by 20% or more (Figure 5b). Increased precipitation does not have a strong effect on melt rates, with only 17% and 9% increase in response to doubled precipitation for Pine Island–Thwaites and Crosson–Dotson, respectively.

Finally, the momentum flux perturbations associated with northward-shifted wind at Pine Island–Thwaites results in intermittent decreases in melt rates, which is noticeable for a 2° northward wind shift (Figure 4c). An extended collapse of basal melting is found over the period 2000–2018 for a northward wind shift of 4.7°. The extended period of low melt rates matches relatively well with those found for reduced precipitation. Crosson–Dotson is again more sensitive, with extended periods of very low melt rates for northward wind shift by 1° or more (Figure 5c). The poleward-shifted winds lead to minor changes in basal melting: less than 5% and 15% increase for Pine Island–Thwaites and Crosson–Dotson, respectively.

We have just shown that abrupt transitions from a permanently high to a permanently low melt state can exist, and we now address the reversibility of these warm-to-cold transitions. We focus on transitions resulting from the strongest perturbations, that is, air cooled by 10°C, precipitation decreased by 52%, and winds shifted northward by 4.7°, and we revert the atmospheric forcing to zero perturbation to re-run the period 1958–2018 starting from the 2018 perturbed state (Figure 3). After 14–21 years, all perturbed melt time series go back to the unperturbed state and remain within ±5% of the original time series (Figure 6). We conclude that all our warm-to-cold transitions in the Amundsen Sea are reversible. This also means that our description of the warm-to-cold transitions can be reverted to describe the cold-to-warm transitions.

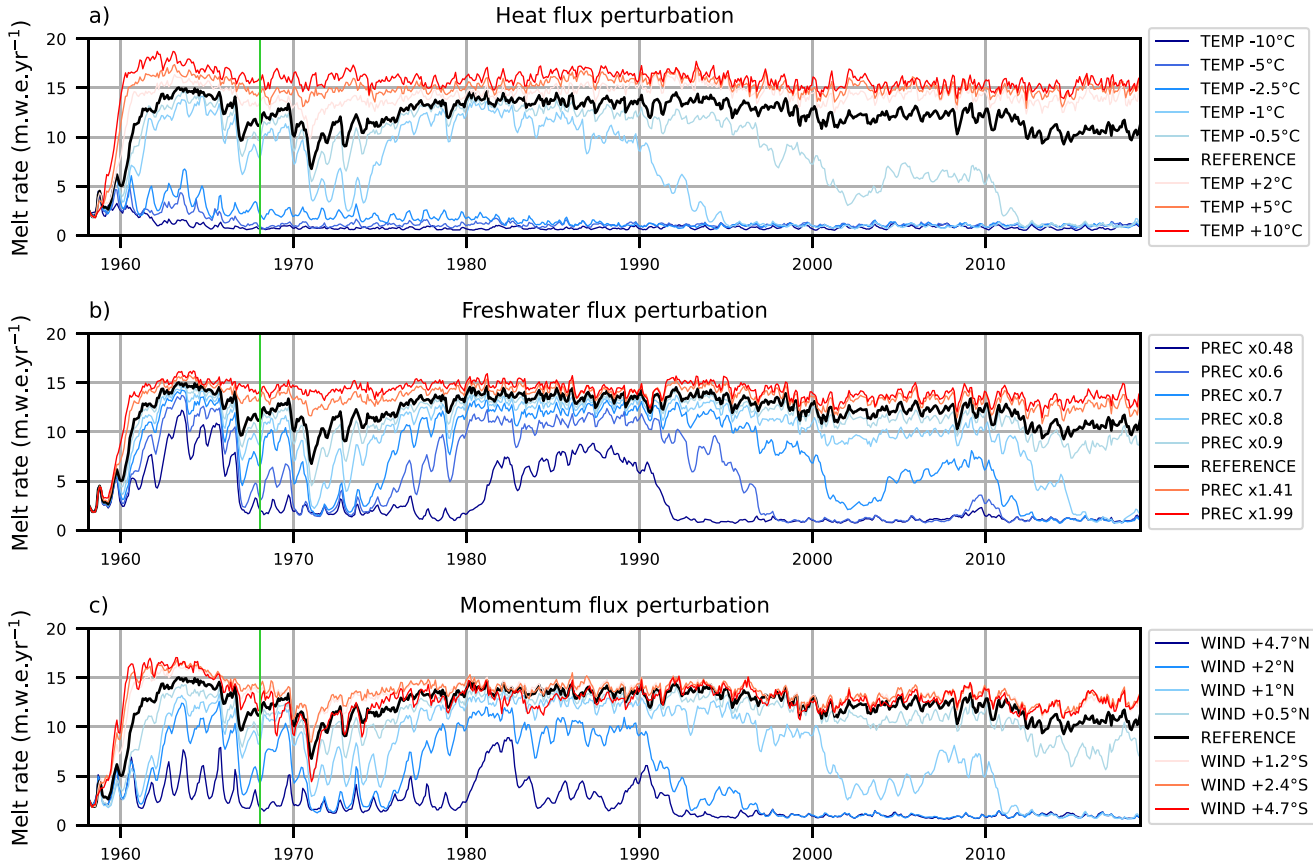

Figure 5. Evolution of monthly basal melting for Crosson and Dotson ice shelves over the period 1958–2018 for perturbations of (a) heat flux, (b) freshwater flux, and (c) momentum flux. The black curve (reference curve) corresponds to the simulation with the JRA55 reanalysis without modification. The red and blue curves correspond to simulations with atmospheric perturbations that aim to increase and decrease basal melting, respectively. The vertical green line indicates the end of the 10-year spin-up.

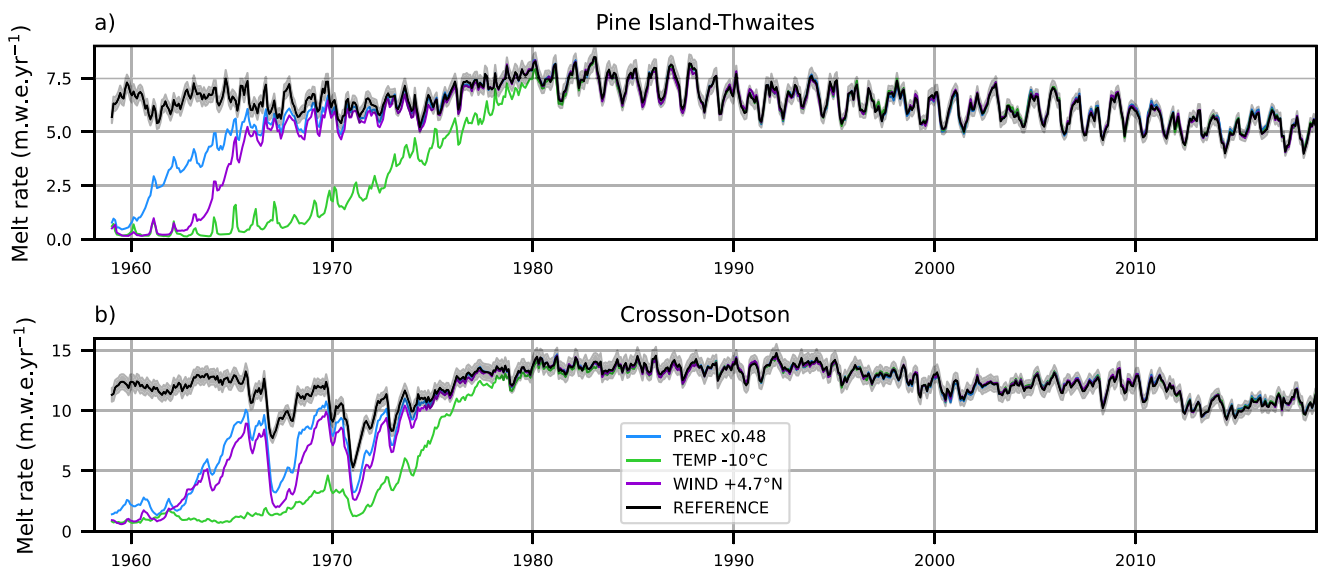

Figure 6. Evolution of the reversed warm-to-cold transition for (a) Pine Island and Thwaites ice shelves and (b) Crosson and Dotson ice shelves. Only the cold-climate perturbations of maximum amplitude are drawn. The black curve corresponds to the simulation driven by the JRA55 reanalysis without modification (natural state), with shading indicating ±5%.

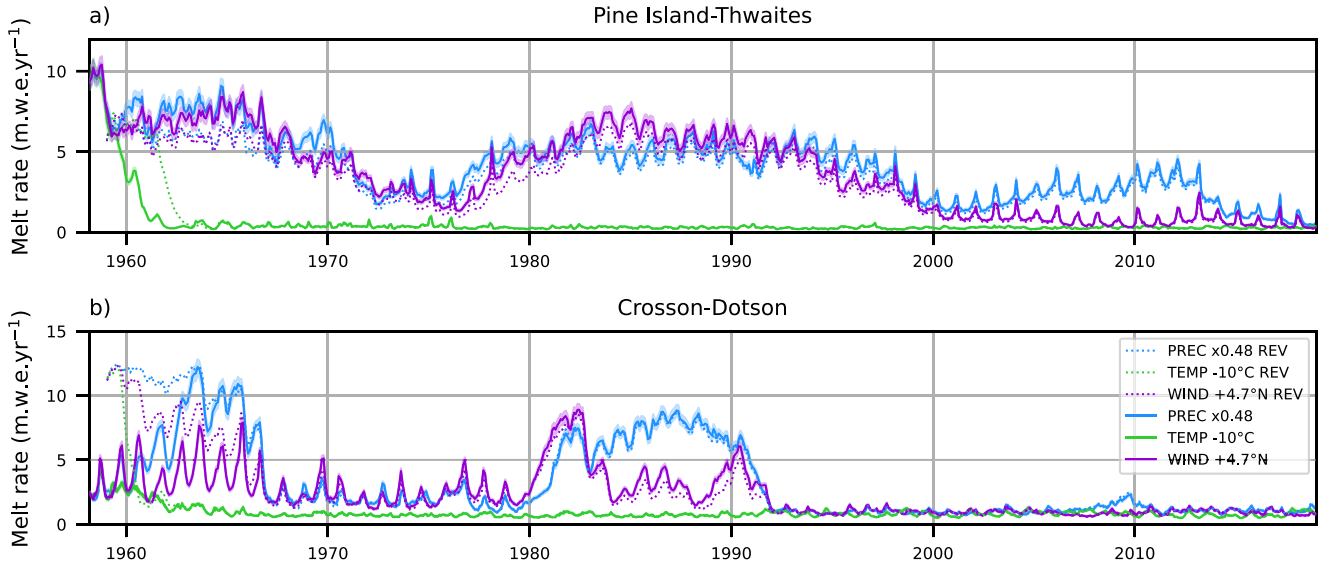

Figure 7. Evolution of the reversed cold-to-warm transition for (a) Pine Island and Thwaites ice shelves and (b) Crosson and Dotson ice shelves. Only the cold-climate perturbations of maximum amplitude are drawn. The solid line represents the melt rate after applying the cold-climate perturbations for the first time over 1958–2018 (first cycle). The dotted line represents the melt rate under the cold-climate perturbations (third cycle) following a 1958–2018 cycle of unperturbed conditions (second cycle). The shading corresponds to the melt value of the perturbed state of the first cycle ±5%.

We also evaluate the reversibility of cold-to-warm transitions, bearing in mind that such transitions may have occurred in the past. To do this, we take the final state of the second cycle of 1958–2018 (unperturbed warm-climate (natural) forcing following a first cold-climate perturbed cycle), and we run a third cycle of 1958–2018 again driven by the cold-climate perturbed forcing (Figure 3). The two perturbed simulations (first and third cycle) converge (within ±5%) after 5–6 years for the perturbed heat flux, after 13–20 years for the perturbed freshwater flux, and after 24–34 years for the perturbed momentum flux (Figure 7). We conclude that the cold-to-warm transitions are also reversible in the Amundsen Sea.

3.2. Physical Processes

From a general perspective, the main external drivers of ocean variations are (a) wind stress changes and (b) surface heat and freshwater fluxes that modify the sea surface buoyancy (e.g., J. Marshall & Plumb, 2008; Talley et al., 2011). Winds induce a tangential stress at the ocean surface (directly or via sea-ice advection) and induce surface water transport perpendicular to the wind due to the balance of the Coriolis effect. This transport results in areas of divergence and convergence at the ocean surface that lead, respectively, to upwelling (Ekman suction) and downwelling (Ekman pumping). Surface heat and freshwater fluxes modify the sea surface buoyancy, which can affect convection and the horizontal circulation via density gradients. At high latitudes, buoyancy variations are mostly driven by salinity changes, which are largely related to net sea-ice production.

Hereafter, we analyze the Ekman vertical velocity (w_{Ek}) and buoyancy flux at the ocean surface (B_s) to assess the impact of atmospheric forcing perturbations on the ocean properties. They are defined as:

$$w_{Ek}\,\vec{k} = \frac{1}{\rho_0}\vec{\nabla}_z \wedge \left(\frac{\vec{\tau}}{f}\right) \tag{3}$$

$$B_s = \frac{g\alpha}{c_p}Q + g\beta S_s F \tag{4}$$

where w_{Ek} is the upward Ekman vertical velocity, ρ_0 the reference seawater density, $\vec{\tau}$ the wind/sea-ice stress at the ocean surface, and f the Coriolis parameter. B_s is the buoyancy flux at the ocean surface, c_p the specific heat, g the gravitational acceleration, S_s the sea surface salinity, α the surface thermal expansion coefficient of seawater, β the corresponding coefficient for salinity, and Q and F are the heat and freshwater fluxes (in units of mass flux) received by the ocean surface (positive downward).

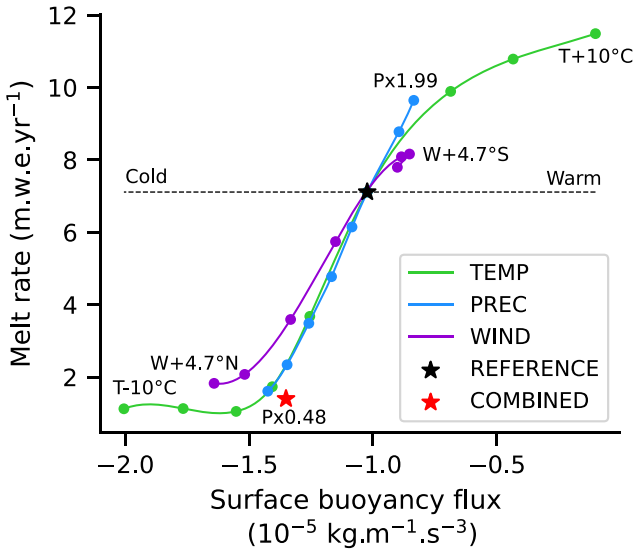

Figure 8. Mean ice-shelf melt rate in the Amundsen Sea as a function of the mean surface buoyancy flux over the Amundsen Sea continental shelf over the period 1988–2018. The green, blue, and purple curves correspond to perturbations of heat, freshwater, and momentum fluxes, respectively. The black star represents the reference case. The red star represents a more realistic case. It corresponds to the current climate −0.5°C by combining the perturbation of all the fluxes (TEMP −0.5°C, PREC ×0.96, and WIND +0.24°N).

A striking feature of our ensemble of experiments is that all types of perturbation approximately have the same ice-shelf melt rate evolution as a function of the surface buoyancy flux over the continental shelf (Figure 8). The evolution curve consists of a highly sensitive regime bounded by a low plateau with no melt variations and a high plateau with lower melt sensitivity. The similarity between the three curves in Figure 8 suggests that all perturbations mostly modify melt rates through changes of the surface buoyancy fluxes. Hereafter, we describe the processes that affect the surface buoyancy for the various types of perturbations.

The freshwater flux perturbations ("PREC" in Figure 8) are the easiest to understand as precipitation directly affects the surface buoyancy. Lowering precipitation reduces the vertical density gradient and thereby favors convective mixing when sea ice is produced (Figure 9c), which extracts the heat of the deep spreading CDW. A much colder water below the thermocline (Figure 9a) explains the lower melt rates in the experiments with reduced precipitation. The opposite mechanism explains higher melt rates in the presence of enhanced precipitation. A small part of the freshwater flux modification is also related to minor changes in net sea-ice production (Figure 10a) due to the additional snow cover, which both increases winter sea-ice production as more snow can be transformed into ice and limits the summer melting as snow plays an insulating role on sea ice (not shown).

The heat flux perturbations ("TEMP" in Figure 8) have a less direct effect on surface buoyancy than just thermal expansion. Modified heat fluxes indeed explain less than 25% of the changes in surface buoyancy fluxes, while changes in freshwater fluxes related to net sea-ice production (i.e., growth minus melt) have a dominant effect on the surface buoyancy fluxes. In the presence of colder air, the net sea-ice production increases considerably over the continental shelf (Figure 10a), mostly due to a drastic decrease in summer melting (not shown). The case is very similar to decreased precipitation, albeit with a larger amplitude: increased convective mixing and related cooling below the thermocline (Figures 9d–9f) leads to reduced ice-shelf melting (Figure 8). Its minimum is reached when the entire water column is close to the surface freezing temperature and the ice-shelf cavities are cold, that is, melt rates are low and only controlled by the pressure dependency of the freezing point. For the warm perturbations, the opposite effect exists until there is too little net sea-ice production (Figure 10a) to induce convective mixing. Beyond that, the CDW layer remains mostly unchanged and ice-shelf melt rates keep increasing only because warmer surface water gets in contact with the ice-shelf base (Figures 9d–9f). This is consistent with the aforementioned increased seasonality of the Pine Island and Thwaites melt rates (Figure 4).

The results of the momentum flux perturbations are probably the most surprising as they affect the surface buoyancy fluxes (see "WIND" in Figure 8), although we have been cautious not to modify the wind field in the calculation of the turbulent heat and evaporation fluxes. The impact of winds on sea-ice drift actually explains the variation in buoyancy flux. In the experiments with a northward wind shift, the net production increases (Figure 10a) as winter sea-ice growth increases and summer melting decreases (not shown), but the sea-ice volume decreases (frozen area and thickness decrease in Figures 10b and 10c). This is explained by enhanced advection of thinner sea ice toward the deep ocean (Figure 11), which leaves space for more air-sea exchange on the continental shelf, that is, more sea-ice production. Therefore, it is a similar perturbation of the vertical ocean stratification as in the case of the freshwater and heat perturbations. In the case of a southward wind shift, the annual sea-ice characteristics are little changed (Figure 10) and so is the mean ice-shelf melt rate (Figure 8).

Our results for the three types of perturbation strongly suggest that buoyancy fluxes are the major driver of ice-shelf basal melt changes. Indeed, the perturbed precipitation experiments, by design, can only be explained by modified surface buoyancy fluxes. The fact that the wind perturbation produces a very similar melt versus buoyancy flux curve strongly suggests that surface buoyancy fluxes explain a large part of the melt response to our wind perturbations. It should also be noted that we have verified that the stress received by the ocean surface

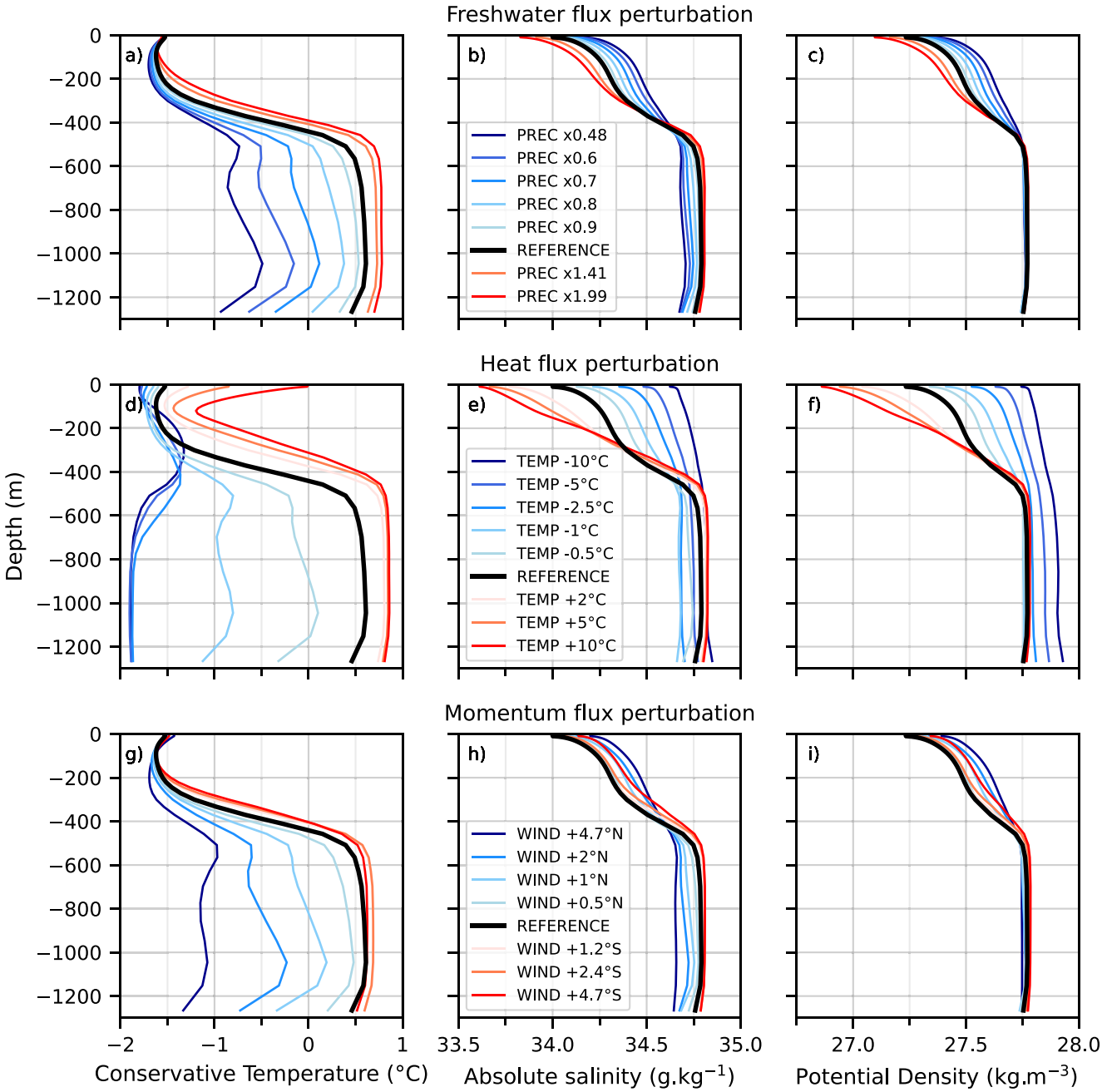

Figure 9. Shelf-averaged vertical profiles of conservative temperature (left), absolute salinity (middle), and potential density (right) over the period 1988–2018 for the various atmospheric perturbations: freshwater flux (top), heat flux (middle), and momentum flux (bottom) perturbations.

at the shelf break is not significantly influenced by modified sea ice properties in the heat and freshwater perturbations (not shown).

So far, we have explained the ocean response to buoyancy fluxes through differences in sea-ice induced convective mixing over the Amundsen Sea continental shelf. We are now going to examine possible connection with the undercurrent flowing eastward, near the sea floor, at the top of the shelf break, and associated with the density gradient of the Antarctic Slope Front (Thompson et al., 2018). This undercurrent has been suggested to bring CDW onto the Amundsen continental shelf (Assmann et al., 2013; Nakayama et al., 2014; Walker et al., 2013) and therefore to modulate ice-shelf melting in response to zonal wind stress variations at the shelf break (Dotto et al., 2020; Kimura et al., 2017).

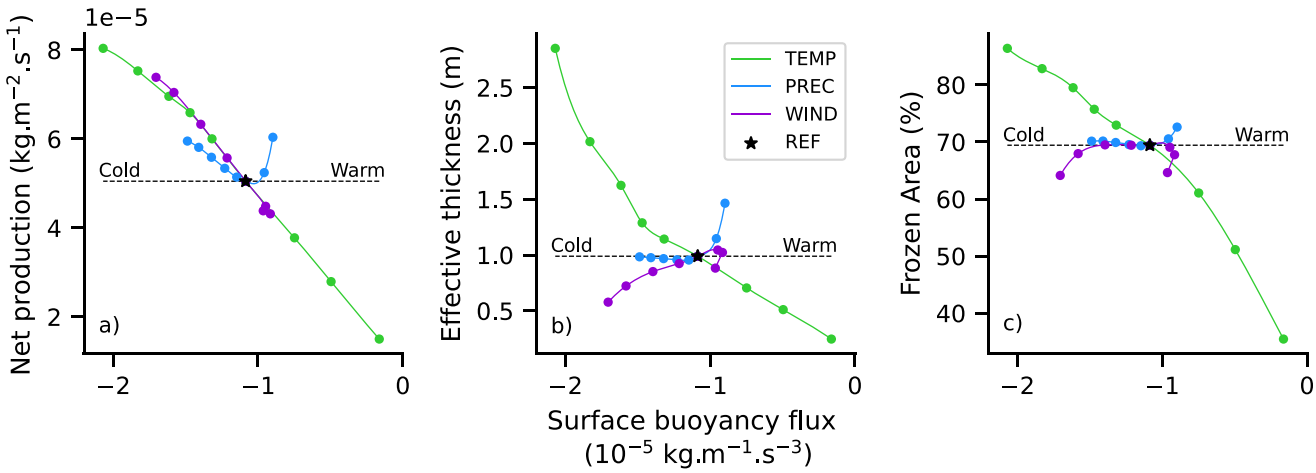

Figure 10. Sea-ice characteristics on the Amundsen Sea continental shelf related to surface buoyancy flux: (a) net production (i.e., growth minus melt), (b) effective thickness (mean thickness over the whole continental shelf including ice-free areas), and (c) frozen area. The star represents the reference case. The perturbed flux configurations are colored in green for heat, blue for freshwater, and purple for momentum.

Our reference simulation contains an Antarctic Slope Front, as can be seen with the isopycnals above the shelf break in Figure 12, and an eastward undercurrent that typically reaches 6 cm s^{-1} (Figure 12). The undercurrent becomes stronger for higher buoyancy fluxes (warm-climate perturbations) and vanishes or reverts for lower buoyancy fluxes (cold-climate perturbations) (Figure 12). A very similar sensitivity is also found at other locations across the shelf break in the Amundsen Sea (not shown). This result is consistent with the vertically-integrated effect of stratification on the geostrophic balance at depth (i.e., the so-called thermal wind). A positive buoyancy flux perturbation on the Amundsen continental shelf (warmer climate) tends to increase the horizontal pressure gradient across the shelf break, which reinforces the eastward undercurrent for any type of perturbation (Figure 12). This mechanism favors CDW inflow and therefore higher ice-shelf melt rates for warm-climate perturbations, while preventing CDW inflow when the undercurrent vanishes or turns westward for cold-climate perturbations.

Ice-shelf melt rates are highly correlated to the undercurrent velocity when the undercurrent flows eastward, and the three types of perturbations follow very similar melt versus undercurrent curves (Figure 13b). The overlap is not as good for melt versus buoyancy fluxes (Figure 8) and for undercurrent velocity versus buoyancy fluxes (Figure 13a): the momentum perturbation has a slightly shifted curve compared to freshwater and heat perturbations. As previously suggested by Kimura et al. (2017) and Dotto et al. (2020), a westward wind anomaly at the shelf break (cold-climate perturbation in Figure 2c) may induce a southward anomaly of Ekman transport near the surface, leading to a southward sea surface height gradient and to a westward anomaly of the barotropic current at the shelf break. Such a barotropic response would further weaken the undercurrent compared to the heat and freshwater perturbations, which is opposite to what we see in Figure 13a. In contrast, the baroclinic mechanism proposed by Silvano et al. (2022) may explain the specificity of the wind perturbation in Figure 13a. A westward wind anomaly at the shelf break would tend to push more surface water toward the continental shelf, which would raise the sea surface and deepen the pycnoclines at depth, thereby reinforcing the undercurrent compared to the heat and freshwater perturbations. The part of the sea surface height and undercurrent modification that is related to wind stress changes is nonetheless difficult to quantify as changes in the distribution of sea ice and surface freshwater fluxes also change sea surface height and isopycnal gradients.

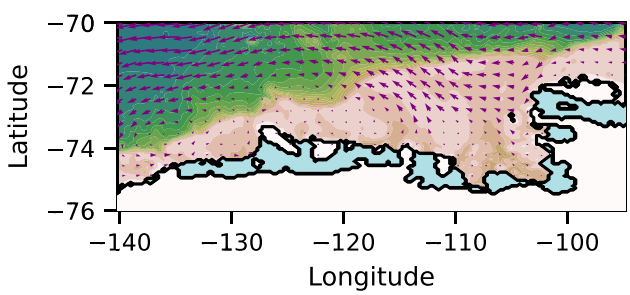

Figure 11. Sea-ice velocity anomaly relative to the reference case for a northward wind shift of 4.7°N. The background map is identical to the one shown in Figure 1.

We also investigated whether changes in Ekman pumping could explain the differences between the momentum perturbation and the two other ones. A downward anomaly of the Ekman velocity (Equation 3) is found on average over the Amundsen continental shelf (not shown), which would tend to decrease the thickness of the CDW layer and to lower ice shelf melt

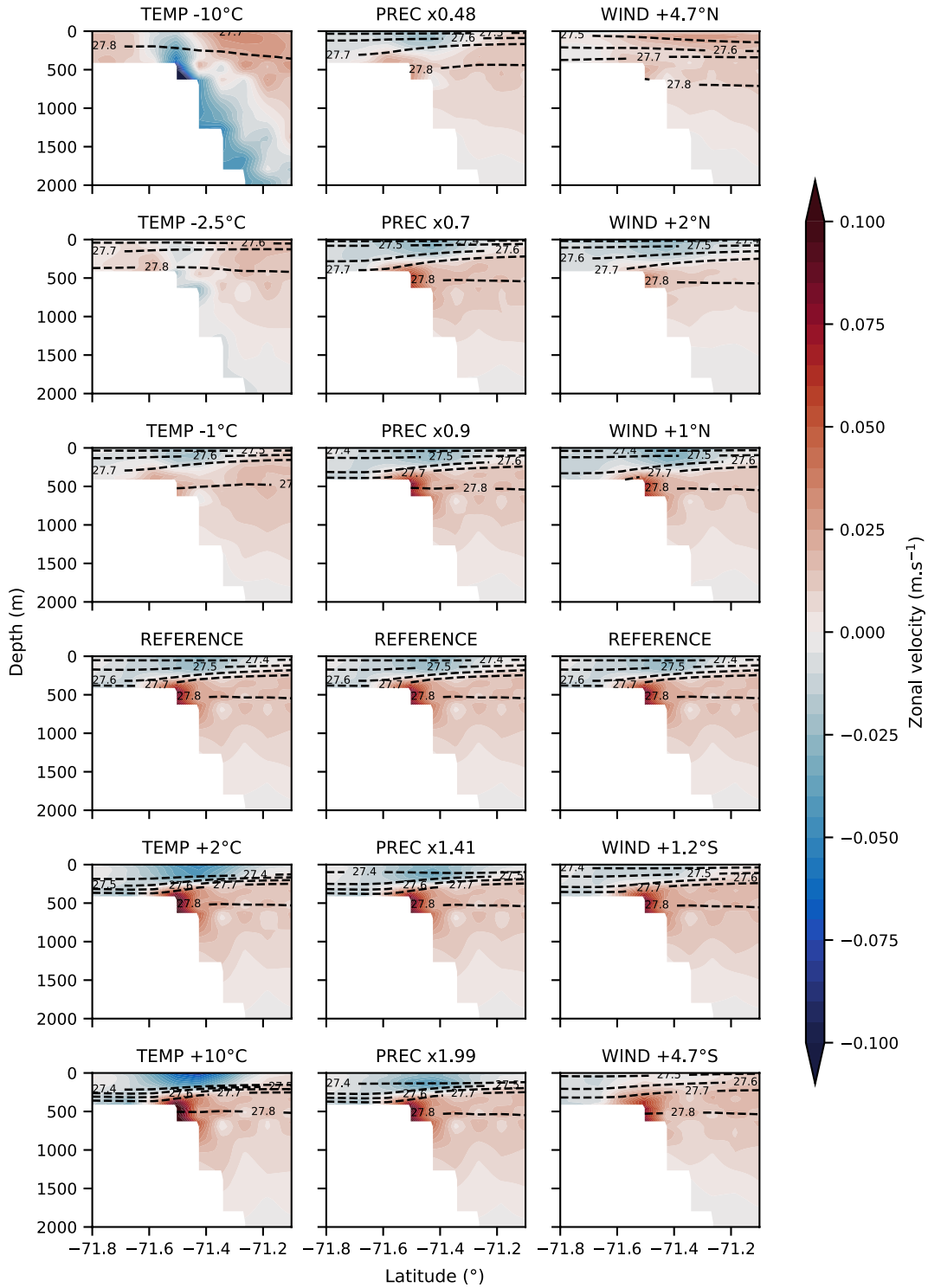

Figure 12. Zonal current velocity (positive eastward) at 115.5°W for several atmospheric perturbations of heat flux (left), freshwater flux (middle), and momentum flux (right). Isopycnals are plotted every 0.1 kg m^{-3}.

rates compared to similar buoyancy fluxes perturbations with unmodified winds. As the opposite is found, we conclude that changes in vertical Ekman velocity at the scale of the continental shelf do not play a key role in the melt response to our idealized perturbations. Similar results were obtained for Ekman pumping averaged in the box defined by Holland et al. (2019), that is, velocity vanishes or reverts at the shelf break (not shown). We also

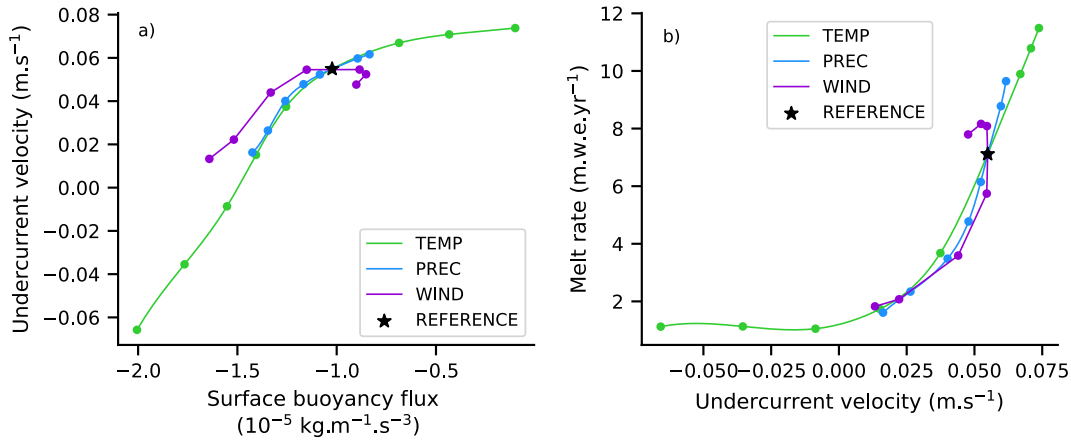

Figure 13. (a) Mean undercurrent velocity (positive eastward) at the shelf break (115°W, 71.43–71.5°S, 420–640 m) as a function of the mean surface buoyancy flux over the Amundsen Sea continental shelf over the period 1988–2018 and (b) mean ice-shelf melt rate in the Amundsen Sea as a function of the mean undercurrent velocity at the shelf break (115°W, 71.43–71.5°S, 420–640 m) over the period 1988–2018. The green, blue, and purple curves correspond to perturbations of heat, freshwater, and momentum fluxes, respectively. The black star represents the reference case.

investigated local anomalies in Ekman vertical velocities following the suggestion by Kim et al. (2021) that it may be important along the Dotson–Getz trough. This did not provide conclusive results, mostly because their high spatial variability (e.g., Figure 2a of Dotto et al., 2019) made it difficult to extract robust diagnostics.

4. Discussion and Conclusion

In this study, we have shown that moderate changes in heat, freshwater, or momentum fluxes can switch the Amundsen Sea to intermittently or permanently cold conditions, with no CDW on the continental shelf and very low ice shelf melt rates. The transitions are reversible, that is, canceling the atmospheric perturbation brings the ocean system back to its unperturbed state within a few decades. Hence, it is possible that the Amundsen Sea underwent a cold-to-warm transition in the past for moderate climate change, but this would not be a proper tipping point in the sense that it is a reversible transition.

Our work emphasizes the importance of surface buoyancy fluxes, which modify the vertical thermohaline stratification on the continental shelf through the modulation of sea-ice induced convection and affect the eastward undercurrent. In warm climate conditions, surface buoyancy fluxes are high, sea-ice convection is limited, and the eastward undercurrent is strong, which gives high ice-shelf melt rates. In cold climate conditions, sea-ice induced convection cools the deep ocean on the continental shelf, while the vanished or reversed undercurrent prevents any intrusion of CDW onto the shelf, which gives very low ice-shelf melt rates.

Hereafter, we discuss the robustness of our results and some implications for past and future climate.

4.1. Robustness of the Thresholds With Respect to Our Model Biases

Our tuned regional model captures well the sea-ice seasonal cycle (Section S3 in Supporting Information S1) and has reasonable biases in mean ocean temperature and salinity profiles (Section S4 in Supporting Information S1). Melt rates exhibit significant biases for individual ice shelves (Section S5 in Supporting Information S1), although of a similar order of magnitude to those found in other regional model studies (e.g., Kimura et al., 2017; Nakayama et al., 2014; Naughten et al., 2022). For an unknown reason, there is almost no interannual variability for Pine Island Ice Shelf in our simulations (Section S7 in Supporting Information S1). The variability observed near and underneath Dotson Ice Shelf is nonetheless well reproduced for relatively small atmospheric perturbations. It should be kept in mind that a small perturbation of 0.5°C of the air temperature is of the order of magnitude of the reanalysis biases estimated by Jones et al. (2016) for the Amundsen Sea region. Biases are also large for precipitation, which is not constrained by data assimilation (Bromwich et al., 2011; Palerme et al., 2017). This means that the "real" Amundsen Sea might correspond to a slightly cooler and drier climate

than our reference state. The melt rate versus buoyancy-flux curve can nonetheless be considered realistic as long as the real state is somewhere on that curve. As the exact air temperature, precipitation, and wind shift thresholds depend on the reference state, there is nonetheless an important uncertainty on the exact value of the thresholds leading to a transition toward a cold state.

4.2. Robustness of the Reversibility of Abrupt Transitions

Our results show that abrupt and reversible warm-to-cold as well as cold-to-warm transitions could occur in the Amundsen Sea for relatively weak regional atmospheric perturbations. The reversibility found in our experiments contrasts with the irreversibility of similar cold-to-warm transitions found in simulations of the Weddell Sea and Filchner-Ronne Ice-Shelf cavity (Comeau et al., 2022; Hazel & Stewart, 2020; Hellmer et al., 2017). The reason why the cold-to-warm transition is reversible in the Amundsen Sea but not in the Weddell Sea remains unclear. The melt-induced circulation was presented as the cause of the irreversibility in Hellmer et al. (2017), but the strong melt-induced circulation in the Amundsen Sea after a cold-to-warm transition (Donat-Magnin et al., 2017; Jourdain et al., 2017) does not seem able to maintain the onshore flow of CDW when the forcing is reverted to cold climate conditions. For the coldest perturbations, the deep Amundsen Sea is approximately at a conservative temperature of -1.9°C and an absolute salinity of 34.7 g kg^{-1} (Figures 9d and 9e), that is, typical of the High Salinity Shelf Water (HSSW) produced in the Weddell Sea. Hazel and Stewart (2020) explain the Weddell Sea tipping point by a feedback of ice-shelf meltwater to the salinity of newly formed HSSW. The tipping conditions and associated hysteresis may, therefore, be sensitive to the ratio between the HSSW formation rate and total ice-shelf basal mass loss, which could explain different regimes in the Weddell and Amundsen Seas.

These transitions and their reversibility may be complicated or facilitated by effects not taken into account in our simulations, such as the feedbacks with the large-scale atmospheric and oceanic circulations or the ice-sheet dynamics.

First of all, we do not change the ocean lateral boundary conditions in our sensitivity experiments, while the Amundsen Sea is also sensitive to changes of water properties advected from remote locations (Nakayama et al., 2018). It is known that large atmospheric changes over multiple decades will have global effects, and we, therefore, acknowledge that our regional point of view is somewhat limited. Furthermore, strong modifications of ice-shelf melting in the Amundsen Sea are expected to have significant consequences at circum-Antarctic (Nakayama et al., 2020) and global scales, with some positive feedback in which more meltwater enhances the stratification and further exposes ice shelves to CDW (Bronselaer et al., 2018; Golledge et al., 2019; Merino et al., 2018). Such feedback is not considered in our study and it is difficult to estimate how they would affect the thresholds and reversibility of our transitions.

Another limitation of our study is the missing evolution of ice-sheet dynamics and iceberg calving in response to changes in ice-shelf melting. In the presence of higher melt rates, ice shelves are expected to thin and their grounding line to retreat. Ice-shelf thinning may slow down melting, if the ice draft raises above the thermocline (De Rydt et al., 2014). Conversely, strong grounding line retreat may enhance melting by exposing a larger basal area to warm water and thus favoring a stronger melt-induced sub-ice shelf circulation (Donat-Magnin et al., 2017). For some geometrical configurations, the retreat of the calving front may also favor melting by facilitating the circulation into ice-shelf cavities (Bradley et al., 2022). If ice-shelf basal melt rates increase sufficiently, the ice dynamics is likely to cross tipping points (Rosier et al., 2021), which would irreversibly put the Amundsen Sea in a different state due to the aforementioned feedback. Nonetheless, it is difficult to quantify the exact thresholds for which irreversibility would be found without using a fully coupled ocean–ice-sheet model.

4.3. Robustness of the Importance of Buoyancy Fluxes Versus Wind Stress

The importance of surface buoyancy fluxes in our results may appear in contradiction with the direct role of wind stress emphasized in previous studies (Dotto et al., 2019; Holland et al., 2019; Naughten et al., 2022; Steig et al., 2012; Thoma et al., 2008; Webber et al., 2019), although there was evidence for an impact of sea-ice formation in some specific years (St-Laurent et al., 2015; Webber et al., 2017) or in simple models (Petty et al., 2013).

We remind that we do suggest a direct melt response to wind stress perturbations (Ekman dynamics), but it appears weaker than the melt response to the associated buoyancy flux perturbations (related to sea ice motions).

Our wind perturbations are nonetheless highly idealized and may not capture the full complexity of wind changes at the continental shelf break. We therefore cannot exclude that more realistic perturbations would lead to a stronger relative importance of wind stress and Ekman dynamics.

It may also be argued that the lack of variability in our reference simulation is an indication that the ocean model is not sensitive enough to wind variations. However, we have previously discussed that a more realistic interannual variability appears near Dotson when the multi-decadal mean buoyancy fluxes are adjusted (although not for Pine Island). We suggest that perturbations over multiple decades slowly modify the horizontal density gradients, which could overwhelm the relatively fast dynamics that directly responds to wind stress perturbations. In other words, interannual variability in ice-shelf melting may well be driven by wind stress and Ekman dynamics, but this variability could be inhibited for too low or too high longer-term surface buoyancy fluxes.

4.4. Implications for Past and Future Climates

Our results indicate cold Amundsen Sea cavities (close to surface freezing point) for conditions typical of the Last Glacial Maximum (Figure 8). This is consistent with grounding lines of paleo-ice streams near the continental shelf break during the last glacial period (Larter et al., 2014). Combined heat, freshwater, and momentum perturbations maintained cold-cavities for climate conditions typical of −0.5°C compared to present day even in the presence of CDW at the continental shelf break (red star in Figure 8). This suggests that preindustrial conditions (approximately 1°C colder than present day; IPCC, 2021) were possibly associated with cold Amundsen Sea and low ice-shelf melt rates, at least intermittently. In ocean–ice-shelf simulations driven by an ensemble of climate simulations following the observed surface variability in the inter-tropical Pacific, Naughten et al. (2022) found that some ensemble members gave similar cold-to-warm transitions, most notably from 1935–1955 to 1960–1965, and to a lower extent from 1975–1985 to 1990–1995. Further work will nonetheless be needed to investigate whether such cold conditions could coexist with ice-shelf edges that remained close to their present-day position for several millennia, as suggested by paleo proxies (Braddock et al., 2022).

The transition from cold to warm cavities may have occurred or be occurring as multi-year oscillations between cold and warm periods (Figures 4 and 5). For conditions warmer than today, the decadal variability is relatively weak and cavities remain permanently warm. Our idealized experiments suggest a gradual but limited increase in ice-shelf basal melting in response to global warming beyond present levels, although some aspects like warming of offshore CDW (Sallée et al., 2013), increased iceberg discharge (Seroussi et al., 2020), or increased iceberg melt rates are not considered in our idealized perturbations.

Data Availability Statement

The model version and set of parameters used to run our experiments are provided in https://doi.org/10.5281/zenodo.7432159. The python scripts used to build the figures are provided in https://doi.org/10.5281/zenodo.7436689 and are mainly based on the Xarray (Hoyer & Hamman, 2017), Numpy (Harris et al., 2020), and Matplotlib (Hunter, 2007) packages.

Acknowledgments
This study was funded by the European Union's Horizon 2020 research and innovation programme under Grant agreement 820575 (TiPACCs) and by the French National Research Agency under Grant ANR-19-CE01-0015 (EIS). This work was granted access to the HPC resources of CINES under the allocation A0100106035 attributed by GENCI. The authors would like to acknowledge Clara Burgard for her valuable advice on figures and presentations as well as Hélène Seroussi for her constructive feedback as a member of the PhD committee.

References

Assmann, K. M., Jenkins, A., Shoosmith, D. R., Walker, D. P., Jacobs, S. S., & Nicholls, K. W. (2013). Variability of circumpolar deep water transport onto the Amundsen Sea Continental shelf through a shelf break trough. *Journal of Geophysical Research: Oceans*, *118*(12), 6603–6620. https://doi.org/10.1002/2013JC008871

Bett, D. T., Holland, P. R., Naveira Garabato, A. C., Jenkins, A., Dutrieux, P., Kimura, S., & Fleming, A. (2020). The impact of the Amundsen Sea freshwater balance on ocean melting of the West Antarctic Ice Sheet. *Journal of Geophysical Research: Oceans*, *125*(9), e2020JC016305. https://doi.org/10.1029/2020jc016305

Braddock, S., Hall, B. L., Johnson, J. S., Balco, G., Spoth, M., Whitehouse, P. L., et al. (2022). Relative sea-level data preclude major late holocene ice-mass change in pine island bay. *Nature Geoscience*, *15*(7), 1–5. https://doi.org/10.1038/s41561-022-00961-y

Bradley, A. T., Bett, D. T., Dutrieux, P., De Rydt, J., & Holland, P. (2022). The influence of Pine Island Ice Shelf calving on basal melting. *JGR Oceans*, *127*(9), e2022JC018621. https://doi.org/10.1029/2022JC018621

Bromwich, D. H., Nicolas, J. P., & Monaghan, A. J. (2011). An assessment of precipitation changes over Antarctica and the southern ocean since 1989 in contemporary global reanalyses. *Journal of Climate*, *24*(16, 4209), 4189–4209. https://doi.org/10.1175/2011jcli4074.1

Bronselaer, B., Winton, M., Griffies, S. M., Hurlin, W. J., Rodgers, K. B., Sergienko, O. V., et al. (2018). Change in future climate due to Antarctic meltwater. *Nature*, *564*(7734), 53–58. https://doi.org/10.1038/s41586-018-0712-z

Brovkin, V., Brook, E., Williams, J. W., Bathiany, S., Lenton, T. M., Barton, M., et al. (2021). Past abrupt changes, tipping points and cascading impacts in the Earth system. *Nature Geoscience*, *14*(8), 550–558. https://doi.org/10.1038/s41561-021-00790-5

Budge, J. S., & Long, D. G. (2018). A comprehensive database for Antarctic iceberg tracking using scatterometer data. *IEEE Journal of Selected Topics in Applied Earth Observations and Remote Sensing*, *11*(2), 434–442. https://doi.org/10.1109/jstars.2017.2784186

Carrère, L., Lyard, F., Cancet, M., Guillot, A., & Roblou, L. (2012). FES2012: A new global tidal model taking advantage of nearly twenty years of altimetry. In *Proceedings of the 20 years of progress in radar altimetry symposium (Venice, Italy)* (pp. 1–20).

Collins, M., Knutti, R., Arblaster, J., Dufresne, J.-L., Fichefet, T., Friedlingstein, P., et al. (2013). Long-term climate change: Projections, commitments and irreversibility. In *Climate change 2013—The physical science basis: Contribution of Working Group I to the Fifth Assessment Report of the Intergovernmental Panel on Climate Change* (pp. 1029–1136). Cambridge University Press.

Comeau, D., Asay-Davis, X. S., Begeman, C. B., Hoffman, M. J., Lin, W., Petersen, M. R., et al. (2022). The DOE E3SM v1.2 cryosphere configuration: Description and simulated Antarctic ice-shelf basal melting. *Journal of Advances in Modeling Earth Systems*, *14*(2), e2021MS002468. https://doi.org/10.1029/2021ms002468

Dekker, M. M., Von Der Heydt, A. S., & Dijkstra, H. A. (2018). Cascading transitions in the climate system. *Earth System Dynamics*, *9*(4), 1243–1260. https://doi.org/10.5194/esd-9-1243-2018

De Rydt, J., Holland, P. R., Dutrieux, P., & Jenkins, A. (2014). Geometric and oceanographic controls on melting beneath pine Island Glacier. *Journal of Geophysical Research: Oceans*, *119*(4), 2420–2438. https://doi.org/10.1002/2013jc009513

Donat-Magnin, M., Jourdain, N. C., Kittel, C., Agosta, C., Amory, C., Gallée, H., et al. (2021). Future surface mass balance and surface melt in the Amundsen sector of the West Antarctic Ice Sheet. *The Cryosphere*, *15*(2), 571–593. https://doi.org/10.5194/tc-15-571-2021

Donat-Magnin, M., Jourdain, N. C., Spence, P., Le Sommer, J., Gallée, H., & Durand, G. (2017). Ice-shelf melt response to changing winds and glacier dynamics in the Amundsen Sea sector, Antarctica. *Journal of Geophysical Research: Oceans*, *122*(12), 10206–10224. https://doi.org/10.1002/2017jc013059

Dotto, T. S., Garabato, A. C., Bacon, S., Holland, P. R., Kimura, S., Firing, Y. L., et al. (2019). Wind-driven processes controlling oceanic heat delivery to the Amundsen Sea, Antarctica. *Journal of Physical Oceanography*, *49*(11), 2829–2849. https://doi.org/10.1175/JPO-D-19-0064.1

Dotto, T. S., Naveira Garabato, A. C., Wåhlin, A. K., Bacon, S., Holland, P. R., Kimura, S., et al. (2020). Control of the oceanic heat content of the Getz-Dotson Trough, Antarctica, by the Amundsen Sea low. *Journal of Geophysical Research: Oceans*, *125*(8). https://doi.org/10.1029/2020JC016113

Durand, G., van den Broeke, M. R., Le Cozannet, G., Edwards, T. L., Holland, P. R., Jourdain, N. C., et al. (2022). Sea-level rise: From global perspectives to local services. *Frontiers in Marine Science*, *8*, 2088. https://doi.org/10.3389/fmars.2021.709595

Favier, L., Durand, G., Cornford, S. L., Gudmundsson, G. H., Gagliardini, O., Gillet-Chaulet, F., et al. (2014). Retreat of Pine Island Glacier controlled by marine ice-sheet instability. *Nature Climate Change*, *4*(2), 117–121. https://doi.org/10.1038/nclimate2094

Garbe, J., Albrecht, T., Levermann, A., Donges, J. F., & Winkelmann, R. (2020). The hysteresis of the Antarctic Ice Sheet. *Nature*, *585*(7826), 538–544. https://doi.org/10.1038/s41586-020-2727-5

Garcia, H. E., Boyer, T. P., Baranova, O. K., Locarnini, R. A., Mishonov, A. V., Grodsky, A., et al. (2019). *World Ocean Atlas 2018: Product documentation*. A. Mishonov, Technical Editor.

Golledge, N. R., Keller, E. D., Gomez, N., Naughten, K. A., Bernales, J., Trusel, L. D., & Edwards, T. L. (2019). Global environmental consequences of twenty-first-century ice-sheet melt. *Nature*, *566*(7742), 65–72. https://doi.org/10.1038/s41586-019-0889-9

Gray, W. R., de Lavergne, C., Wills, R. C., Menviel, L., Spence, P., Holzer, M., et al. (2021). Poleward shift in the southern hemisphere westerly winds synchronous with the deglacial rise in CO_2. *Earth ArXiv*. https://doi.org/10.31223/X5P02C

Griffies, S. M., Biastoch, A., Böning, C., Bryan, F., Danabasoglu, G., Chassignet, E. P., et al. (2009). Coordinated Ocean-ice Reference Experiments (COREs). *Ocean Modelling*, *26*(1–2), 1–46. https://doi.org/10.1016/j.ocemod.2008.08.007

Gudmundsson, G. H. (2013). Ice-shelf buttressing and the stability of marine ice sheets. *The Cryosphere*, *7*(2), 647–655. https://doi.org/10.5194/tc-7-647-2013

Harris, C. R., Millman, K. J., van der Walt, S. J., Gommers, R., Virtanen, P., Cournapeau, D., et al. (2020). Array programming with NumPy. *Nature*, *585*(7825), 357–362. https://doi.org/10.1038/s41586-020-2649-2

Hazel, J. E., & Stewart, A. L. (2020). Bistability of the Filchner-Ronne Ice Shelf cavity circulation and basal melt. *Journal of Geophysical Research: Oceans*, *125*(4), e2019JC015848. https://doi.org/10.1029/2019jc015848

Hellmer, H. H., Kauker, F., Timmermann, R., Determann, J., & Rae, J. (2012). Twenty-first-century warming of a large Antarctic ice-shelf cavity by a redirected coastal current. *Nature*, *485*(7397), 225–228. https://doi.org/10.1038/nature11064

Hellmer, H. H., Kauker, F., Timmermann, R., & Hattermann, T. (2017). The fate of the Southern Weddell sea continental shelf in a warming climate. *Journal of Climate*, *30*(12), 4337–4350. https://doi.org/10.1175/JCLI-D-16-0420.1

Hinkel, J., Church, J. A., Gregory, J. M., Lambert, E., Le Cozannet, G., Lowe, J., et al. (2019). Meeting user needs for sea level rise information: A decision analysis perspective. *Earth's Future*, *7*(3), 320–337. https://doi.org/10.1029/2018EF001071

Holland, P. R., Bracegirdle, T. J., Dutrieux, P., Jenkins, A., & Steig, E. J. (2019). West Antarctic ice loss influenced by internal climate variability and anthropogenic forcing. *Nature Geoscience*, *12*(9), 718–724. https://doi.org/10.1038/s41561-019-0420-9

Hoyer, S., & Hamman, J. (2017). xarray: N-D labeled arrays and datasets in Python. *Journal of Open Research Software*, *5*(1), 10. https://doi.org/10.5334/jors.148

Hunter, J. D. (2007). Matplotlib: A 2D graphics environment. *Computing in Science & Engineering*, *9*(3), 90–95. https://doi.org/10.1109/MCSE.2007.55

IPCC. (2021). Climate change 2021: The physical science basis. In V. Masson-Delmotte, P. Zhai, A. Pirani, S. L. Connors, C. Péan, S. Berger, et al. (Eds.), *Contribution of working group I to the sixth assessment report of the intergovernmental panel on climate change* (Vol. 2). Cambridge University Press. Cambridge, UK.

Jacobs, S., Jenkins, A., Hellmer, H., Giulivi, C., Nitsche, F., Huber, B., & Guerrero, R. (2012). *The Amundsen Sea and the Antarctic ice sheet*. *Oceanography*, 25(3), 154–163. https://doi.org/10.5670/oceanog.2012.90

Jacobs, S., Hellmer, H. H., & Jenkins, A. (1996). Antarctic ice sheet melting in the southeast Pacific. *Geophysical Research Letters*, *23*(9), 957–960. https://doi.org/10.1029/96gl00723

Jenkins, A., Shoosmith, D., Dutrieux, P., Jacobs, S., Kim, T. W., Lee, S. H., et al. (2018). West Antarctic Ice Sheet retreat in the Amundsen Sea driven by decadal oceanic variability. *Nature Geoscience*, *11*(10), 733–738. https://doi.org/10.1038/s41561-018-0207-4

Jones, R. W., Renfrew, I. A., Orr, A., Webber, B. G., Holland, D. M., & Lazzara, M. A. (2016). Evaluation of four global reanalysis products using in situ observations in the Amundsen Sea embayment, Antarctica. *Journal of Geophysical Research*, *121*(11), 6240–6257. https://doi.org/10.1002/2015JD024680

Joughin, I., Smith, B. E., & Medley, B. (2014). Marine ice sheet collapse potentially under way for the Thwaites Glacier basin, West Antarctica. *Science*, *344*(6185), 735–738. https://doi.org/10.1126/science.1249055

Jourdain, N. C., Mathiot, P., Merino, N., Durand, G., Le Sommer, J., Spence, P., et al. (2017). Ocean circulation and sea-ice thinning induced by melting ice shelves in the Amundsen Sea. *Journal of Geophysical Research: Oceans*, *122*(3), 2550–2573. https://doi.org/10.1002/2016JC012509

Jourdain, N. C., Molines, J. M., Le Sommer, J., Mathiot, P., Chanut, J., de Lavergne, C., & Madec, G. (2019). Simulating or prescribing the influence of tides on the Amundsen Sea ice shelves. *Ocean Modelling*, *133*, 44–55. https://doi.org/10.1016/j.ocemod.2018.11.001

Kim, T. W., Yang, H. W., Dutrieux, P., Wåhlin, A. K., Jenkins, A., Kim, Y. G., et al. (2021). Interannual variation of modified circumpolar deep water in the Dotson-Getz trough, West Antarctica. *Journal of Geophysical Research: Oceans*, *126*(12). e2021JC017491. https://doi.org/10.1029/2021JC017491

Kimura, S., Jenkins, A., Regan, H., Holland, P. R., Assmann, K. M., Whitt, D. B., et al. (2017). Oceanographic controls on the variability of ice-shelf basal melting and circulation of glacial meltwater in the Amundsen Sea Embayment, Antarctica. *Journal of Geophysical Research: Oceans*, *122*(12), 10131–10155. https://doi.org/10.1002/2017jc012926

Large, W. G., & Yeager, S. G. (2004). *Diurnal to decadal global forcing for ocean and sea-ice models: The data sets and flux climatologies*. Citeseer.

Larter, R. D., Anderson, J. B., Graham, A. G., Gohl, K., Hillenbrand, C. D., Jakobsson, M., et al. (2014). Reconstruction of changes in the Amundsen Sea and Bellingshausen Sea sector of the West Antarctic Ice Sheet since the last glacial maximum. *Quaternary Science Reviews*, *100*, 55–86. https://doi.org/10.1016/j.quascirev.2013.10.016

Lee, J.-Y., Marotzke, J., Bala, G., Cao, L., Corti, S., Dunne, J. P., et al. (2021). *Future global climate: Scenario-based projections and near-term information*. IPCC.

Ligtenberg, S. R., van de Berg, W. J., van den Broeke, M. R., Rae, J. G., & van Meijgaard, E. (2013). Future surface mass balance of the Antarctic ice sheet and its influence on sea level change, simulated by a regional atmospheric climate model. *Climate Dynamics*, *41*(3–4), 867–884. https://doi.org/10.1007/s00382-013-1749-1

Lindsey, A. A. (1995). The exploration history of the Lindsey Islands, Antarctica, 1928–1994. *Proceedings of the Indiana Academy of Science*, *104*, 85–92.

Lyard, F., Lefevre, F., Letellier, T., & Francis, O. (2006). Modelling the global ocean tides: Modern insights from FES2004. *Ocean Dynamics*, *56*(5–6), 394–415. https://doi.org/10.1007/s10236-006-0086-x

Madec, G., & NEMO-Team. (2016). Note du Pôle de modélisation de l'Institut Pierre-Simon Laplace No 27. In *NEMO ocean engine, version 3.6 stable (Technical Report)*. France: IPSL.

Marshall, G. J., Fogt, R. L., Turner, J., & Clem, K. R. (2022). Can current reanalyses accurately portray changes in southern annular mode structure prior to 1979? Climate Dynamics, *59*(11–12), 1–24. https://doi.org/10.1007/s00382-022-06292-3

Marshall, J., & Plumb, R. A. (2008). *Atmosphere, ocean, and climate dynamics*. Elsevier.

Masson-Delmotte, V., Stenni, B., Pol, K., Braconnot, P., Cattani, O., Falourd, S., et al. (2010). EPICA Dome C record of glacial and interglacial intensities. *Quaternary Science Reviews*, *29*(1–2), 113–128. https://doi.org/10.1016/j.quascirev.2009.09.030

Mathiot, P., Jenkins, A., Harris, C., & Madec, G. (2017). Explicit representation and parametrised impacts of under ice shelf seas in the z*-coordinate ocean model NEMO 3.6. *Geoscientific Model Development*, *10*(7), 2849–2874. https://doi.org/10.5194/gmd-10-2849-2017

Matsuoka, K., Skoglund, A., Roth, G., de Pomereu, J., Griffiths, H., Headland, R., et al. (2021). Quantarctica, an integrated mapping environment for Antarctica, the Southern Ocean, and sub-Antarctic islands. *Environmental Modelling & Software*, *140*, 105015. https://doi.org/10.1016/j.envsoft.2021.105015

Mazur, A., Wåhlin, A. K., & Krežel, A. (2017). An object-based SAR image iceberg detection algorithm applied to the Amundsen Sea. *Remote Sensing of Environment*, *189*, 67–83. https://doi.org/10.1016/j.rse.2016.11.013

Merino, N., Jourdain, N. C., Le Sommer, J., Goosse, H., Mathiot, P., & Durand, G. (2018). Impact of increasing Antarctic glacial freshwater release on regional sea-ice cover in the Southern Ocean. *Ocean Modelling*, *121*, 76–89. https://doi.org/10.1016/j.ocemod.2017.11.009

Merino, N., Le Sommer, J., Durand, G., Jourdain, N. C., Madec, G., Mathiot, P., & Tournadre, J. (2016). Antarctic icebergs melt over the Southern Ocean: Climatology and impact on sea ice. *Ocean Modelling*, *104*, 99–110. https://doi.org/10.1016/j.ocemod.2016.05.001

Morlighem, M., Rignot, E., Binder, T., Blankenship, D., Drews, R., Eagles, G., et al. (2020). Deep glacial troughs and stabilizing ridges unveiled beneath the margins of the Antarctic ice sheet. *Nature Geoscience*, *13*(2), 132–137. https://doi.org/10.1038/s41561-019-0510-8

Nakayama, Y., Menemenlis, D., Zhang, H., Schodlok, M., & Rignot, E. (2018). Origin of circumpolar deep water intruding onto the Amundsen and Bellingshausen Sea continental shelves. *Nature Communications*, *9*(1), 3403. https://doi.org/10.1038/s41467-018-05813-1

Nakayama, Y., Timmermann, R., & Hellmer, H. (2020). Impact of west Antarctic ice shelf melting on southern ocean hydrography. *The Cryosphere*, *14*(7), 2205–2216. https://doi.org/10.5194/tc-14-2205-2020

Nakayama, Y., Timmermann, R., Schröder, M., & Hellmer, H. H. (2014). On the difficulty of modeling circumpolar deep water intrusions onto the Amundsen Sea continental shelf. *Ocean Modelling*, *84*, 26–34. https://doi.org/10.1016/j.ocemod.2014.09.007

Naughten, K. A., Holland, P. R., Dutrieux, P., Kimura, S., Bett, D. T., & Jenkins, A. (2022). Simulated twentieth-century ocean warming in the Amundsen Sea, West Antarctica. *Geophysical Research Letters*, *49*(5), e2021GL094566. https://doi.org/10.1029/2021gl094566

Palerme, C., Claud, C., Dufour, A., Genthon, C., Wood, N. B., & L'Ecuyer, T. (2017). Evaluation of Antarctic snowfall in global meteorological reanalyses. *Atmospheric Research*, *190*, 104–112. https://doi.org/10.1016/j.atmosres.2017.02.015

Pattyn, F., Schoof, C., Perichon, L., Hindmarsh, R. C., Bueler, E., De Fleurian, B., et al. (2012). Results of the marine ice sheet model intercomparison project, MISMIP. *Cryosphere*, *6*(3), 573–588. https://doi.org/10.5194/tc-6-573-2012

Petty, A. A., Feltham, D. L., & Holland, P. R. (2013). Impact of atmospheric forcing on Antarctic continental shelf water masses. *Journal of Physical Oceanography*, *43*(5), 920–940. https://doi.org/10.1175/jpo-d-12-0172.1

Rignot, E., Jacobs, S., Mouginot, J., & Scheuchl, B. (2013). Ice-shelf melting around Antarctica. *Science*, *341*(6143), 266–270. https://doi.org/10.1126/science.1235798

Rosier, S. H., Reese, R., Donges, J. F., De Rydt, J., Hilmar Gudmundsson, G., & Winkelmann, R. (2021). The tipping points and early warning indicators for Pine Island Glacier, West Antarctica. *The Cryosphere*, *15*(3), 1501–1516. https://doi.org/10.5194/tc-15-1501-2021

Rousset, C., Vancoppenolle, M., Madec, G., Fichefet, T., Flavoni, S., Barthélemy, A., et al. (2015). The Louvain-La-Neuve sea ice model LIM3.6: Global and regional capabilities. *Geoscientific Model Development*, *8*(10), 2991–3005. https://doi.org/10.5194/gmd-8-2991-2015

Sallée, J. B., Shuckburgh, E., Bruneau, N., Meijers, A. J., Bracegirdle, T. J., Wang, Z., & Roy, T. (2013). Assessment of southern ocean water mass circulation and characteristics in CMIP5 models: Historical bias and forcing response. *Journal of Geophysical Research: Oceans*, *118*(4), 1830–1844. https://doi.org/10.1002/jgrc.20135

Schoof, C. (2007). Marine ice-sheet dynamics. Part 1. The case of rapid sliding. *Journal of Fluid Mechanics*, *573*, 27–55. https://doi.org/10.1017/S0022112006003570

Seroussi, H., Nowicki, S., Payne, A. J., Goelzer, H., Lipscomb, W. H., Abe-Ouchi, A., et al. (2020). ISMIP6 Antarctica: A multi-model ensemble of the Antarctic ice sheet evolution over the 21st century. *The Cryosphere*, *14*(9), 3033–3070. https://doi.org/10.5194/tc-14-3033-2020

Silvano, A., Holland, P. R., Naughten, K. A., Dragomir, O., Dutrieux, P., Jenkins, A., et al. (2022). Baroclinic ocean response to climate forcing regulates decadal variability of ice-shelf melting in the Amundsen Sea. *Geophysical Research Letters*, *49*(24). e2022GL100646. https://doi.org/10.1029/2022gl100646

Smith, J. A., Andersen, T. J., Shortt, M., Gaffney, A. M., Truffer, M., Stanton, T. P., et al. (2017). Sub-ice-shelf sediments record history of twentieth-century retreat of Pine Island Glacier. *Nature*, *541*(7635), 77–80. https://doi.org/10.1038/nature20136

Spence, P., Griffies, S. M., England, M. H., Hogg, A. M. C., Saenko, O. A., & Jourdain, N. C. (2014). Rapid subsurface warming and circulation changes of Antarctic coastal waters by poleward shifting winds. *Geophysical Research Letters*, *41*(13), 4601–4610. https://doi.org/10.1002/2014GL060613

Steig, E. J., Ding, Q., Battisti, D. S., & Jenkins, A. (2012). Tropical forcing of circumpolar deep water inflow and outlet glacier thinning in the Amundsen Sea embayment, west Antarctica. *Annals of Glaciology*, *53*(60), 19–28. https://doi.org/10.3189/2012aog60a110

St-Laurent, P., Klinck, J., & Dinniman, M. (2015). Impact of local winter cooling on the melt of Pine Island Glacier, Antarctica. *Journal of Geophysical Research: Oceans*, *120*(10), 6718–6732. https://doi.org/10.1002/2015jc010709

Talley, L. D., Pickard, G. L., Emery, W. J., & Swift, J. H. (2011). Descriptive physical oceanography: An introduction (6th ed.). https://doi.org/10.1016/C2009-0-24322-4

Thoma, M., Jenkins, A., Holland, D., & Jacobs, S. (2008). Modelling circumpolar deep water intrusions on the Amundsen Sea continental shelf, Antarctica. *Geophysical Research Letters*, *35*(18), L18602. https://doi.org/10.1029/2008gl034939

Thompson, A. F., Stewart, A. L., Spence, P., & Heywood, K. J. (2018). The Antarctic slope current in a changing climate. *Reviews of Geophysics*, *56*(4), 741–770. https://doi.org/10.1029/2018RG000624

Tournadre, J., Bouhier, N., Girard-Ardhuin, F., & Rémy, F. (2015). Large icebergs characteristics from altimeter waveforms analysis. *Journal of Geophysical Research: Oceans*, *120*(3), 1954–1974. https://doi.org/10.1002/2014jc010502

Tsujino, H., Urakawa, S., Nakano, H., Small, R. J., Kim, W. M., Yeager, S. G., et al. (2018). JRA-55 based surface dataset for driving ocean–sea-ice models (JRA55-do). *Ocean Modelling*, *130*, 79–139. https://doi.org/10.1016/j.ocemod.2018.07.002

Turney, C. S., Fogwill, C. J., Golledge, N. R., McKay, N. P., van Sebille, E., Jones, R. T., et al. (2020). Early last interglacial ocean warming drove substantial ice mass loss from Antarctica. *Proceedings of the National Academy of Sciences*, *117*(8), 3996–4006. https://doi.org/10.1073/pnas.1902469117

Walker, D. P., Jenkins, A., Assmann, K. M., Shoosmith, D. R., & Brandon, M. A. (2013). Oceanographic observations at the shelf break of the Amundsen Sea, Antarctica. *Journal of Geophysical Research: Oceans*, *118*(6), 2906–2918. https://doi.org/10.1002/jgrc.20212

Webber, B. G., Heywood, K. J., Stevens, D. P., & Assmann, K. M. (2019). The impact of overturning and horizontal circulation in Pine Island trough on ice shelf melt in the eastern Amundsen Sea. *Journal of Physical Oceanography*, *49*(1), 63–83. https://doi.org/10.1175/JPO-D-17-0213.1

Webber, B. G., Heywood, K. J., Stevens, D. P., Dutrieux, P., Abrahamsen, E. P., Jenkins, A., et al. (2017). Mechanisms driving variability in the ocean forcing of Pine Island Glacier. *Nature Communications*, *8*(1), 14507. https://doi.org/10.1038/ncomms14507

Wunderling, N., Donges, J. F., Kurths, J., & Winkelmann, R. (2021). Interacting tipping elements increase risk of climate domino effects under global warming. *Earth System Dynamics*, *12*(2), 601–619. https://doi.org/10.5194/esd-12-601-2021